Jian Pi Sheng Sui Gao (JPSSG) alleviation of skeletal myoblast cell apoptosis, oxidative stress, and mitochondrial dysfunction to improve cancer-related fatigue in an AMPK-SIRT1- and HIF-1-dependent manner

Min Xiao[1,2#], Wei Guo[1#], Chi Zhang[1], Yukun Zhu[3], Zhiling Li[2], Cui Shao[1], Jiling Jiang[4], Zhenjiang Yang[5], Jianyong Zhang[2], Lizhu Lin[1]

[1]Clinical Discipline of Integrated Chinese and Western Medicine, The First Clinical Medical College of Guangzhou University of Chinese Medicine, Guangzhou, China; [2]Department of Rheumatology, Shenzhen Traditional Chinese Medicine Hospital, Shenzhen, China; [3]Department of Science and Education, Shenzhen Traditional Chinese Medicine Hospital, Shenzhen, China; [4]Department of General Surgery, Shenzhen Traditional Chinese Medicine Hospital, Shenzhen, China; [5]Department of Oncology and Hematology, Shenzhen Traditional Chinese Medicine Hospital, Shenzhen, China

Contributions: (I) Conception and design: L Lin; (II) Administrative support: None; (III) Provision of study materials or patients: M Xiao, W Guo, C Zhang; (IV) Collection and assembly of data: Y Zhu, Z Li, C Shao, J Jiang; (V) Data analysis and interpretation: Z Yang, J Zhang; (VI) Manuscript writing: All authors; (VII) Final approval of manuscript: All authors.

[#]These authors contributed equally to this work.

Correspondence to: Lizhu Lin, MD. Clinical Discipline of Integrated Chinese and Western Medicine, The First Clinical Medical College, Guangzhou University of Chinese Medicine, No. 12 Jichang Road, Sanyuanli, Guangzhou 510405, China. Email: linlizhu@gzucm.edu.cn.

Background: Jian Pi Sheng Sui Gao (JPSSG), a Chinese traditional herbal paste, possesses certain efficacy in patients with cancer-related fatigue (CRF); however, its related mechanism remains unclear. Hence, network pharmacology analysis, followed by *in vivo* and *in vitro* experiments were conducted in this study with the aim to evaluate the effect of JPSSG on CRF and clarify its potential mechanism.

Methods: Network pharmacology analysis was performed. Subsequently, 12 mice were injected with CT26 cells to establish CRF mouse models and randomly divided into a model group (n=6) and JPSSG group (n=6); meanwhile, another 6 normal mice served as a control group. Then, 3.0 g/kg JPSSG was given to mice in JPSSG group for 15 days, while mice in the n control and model groups received phosphate-buffered saline (PBS) of the same volume for 15 days. For the *in vitro* experiment, CT26 conditioned medium (CM) was established; meanwhile, the mitochondrial damage model was constructed through C2C12 myotubes stimulated with H_2O_2. C2C12 myotubes were divided into 5 groups: control group (without treatment), CM group, CM + JPSSG group, H_2O_2 group, and H_2O_2 + JGSSP group.

Results: Network pharmacology analysis identified 87 bioactive compounds and 132 JPSSG-CRF interaction targets. Moreover, according to the Kyoto Encyclopedia of Genes and Genomes enrichment analysis and the subsequent *in vivo* and *in vitro* experiments, JPSSG activated adenosine 5'-monophosphate-activated protein kinase-silent-information-regulator factor 2-related-enzyme 1 (AMPK-SIRT1) and hypoxia-inducible factor-1 (HIF-1) signaling pathways during CRF. Moreover, the *in vivo* experiment showed that JPSSG attenuated CRF in mice, reflected by increased distance traveled, mobile time in open field test, and swimming time in exhaustive swimming test, and decreased absolute rest time and tail suspension test in the JPSSG group (*vs.* model group). Furthermore, JPSSG upregulated gastrocnemius weight, adenosine triphosphate (ATP), superoxide dismutase (SOD), and the cross-sectional area of the gastrocnemius. With regard to *in vitro* study, JPSSG elevated cell viability, B-cell lymphoma-2, ATP, SOD, and mitochondrial membrane potential, while it decreased apoptosis rate, cleaved-caspase3, malondialdehyde, and reactive oxygen species in C2C12 myotubes.

Conclusions: JPSSG ameliorates CRF via alleviating skeletal myoblast cell apoptosis, oxidative stress, and mitochondrial dysfunction in an AMPK-SIRT1- and HIF-1-dependent manner.

Keywords: Jian Pi Sheng Sui Gao (JPSSG); cancer-related fatigue (CRF); network pharmacology; molecular mechanism; oxidative stress

Introduction

Cancer-related fatigue (CRF), which is induced by the cancer itself or cancer-related treatment, is a kind of physical, emotional, or cognitive fatigue (1-3). The incidence of CRF varies across different reports (ranging from 14.0% to 100.0%) due to the different regions, cancer types, and assessment methods in each study (4-6). Concerning the complex pathobiology of CRF, previous evidences indicate that mitochondria modulate several cellular processes (including the production of reactive oxygen species, cell damage, energy production, etc.), leading to skeletal muscle dysfunction and further CRF initiation (7,8). Worryingly, patients with CRF can only gain minimal relief through simple rest, and thus their fatigue symptoms are constant and further disturb their quality of life (9,10). At present, various interventions have been developed for relieving CRF (such as exercise interventions, psychosomatic therapies, psychoeducation, etc.), while there still lacks standardized treatment (11). Additionally, CRF is a leading reason why those with cancer abandon subsequent

treatment, which greatly interferes with their prognosis (12). Thus, finding efficient interventions to treat CRF would be helpful for improving the clinical outcomes of patients with cancer.

Jian Pi Sheng Sui Gao (JPSSG), a Chinese traditional herbal paste, consists of 17 kinds of herbs (including *Chinemys reevesii*, *Cervus elaphus*, *Ligustrum lucidum*, *Codonopsis*, *Hordeum vulgare*, *Citrus reticulata*, *Lycium barbarum*, etc.) (13). Several studies have explored the pleasing treatment efficacy of JPSSG in patients with CRF (14-16). For instance, one study noted the good efficacy of JPSSG to treat CRF in patients with lung cancer, reflected by the declined Piper fatigue scale (PFS) and traditional Chinese medicine (TCM) symptom score in patients who received JPSSG plus chemotherapy (*vs.* chemotherapy alone) (15). Another study also reported that the CRF degree was ameliorated in patients with cancer who received JPSSG combined with chemotherapy (*vs.* chemotherapy alone) (14). Nevertheless, although the aforementioned studies supported the clinical efficacy of JPSSG in treating CRF, the underlying mechanism of its effect remains unknown. Network pharmacology analysis, an appropriate approach for modern TCM research, utilizes high-throughput screening analysis and network database retrieval techniques to reveal the network relationship of drug-gene-target-disease interaction (17).

Therefore, network pharmacology analysis, followed by *in vivo* and *in vitro* experiments were conducted in this study, aiming to explore the effect of JPSSG on CRF and its potential mechanism. We present the following article in accordance with the ARRIVE reporting checklist (available at https://atm.amegroups.com/article/view/10.21037/atm-22-6611/rc).

Methods

Network pharmacology analysis of JPSSG

The compounds of the JPSSG were retrieved from the

Highlight box

Key findings
- JPSSG alleviates skeletal myoblast cell apoptosis, oxidative stress, and mitochondrial dysfunction via AMPK-SIRT1 and HIF-1 to relieve CRF.

What is known and what is new?
- JPSSG possesses good treatment efficacy in patients with CRF.
- This study clarified the potential mechanism of JPSSG in treating CRF through network pharmacology, *in vivo*, and *in vitro* experiments.

What is the implication, and what should change now?
- This study outlines the potential mechanism of JPSSG and provides theoretical evidence for its clinical application; however, for a more detailed understanding of this molecular mechanism further exploration and verification in future study are required.

Traditional Chinese Medicine Systems Pharmacology Database (TCMSP) of traditional Chinese medicine as previously described (18). A drug likeness (DL) ≥0.18, oral bioavailability (OB) ≥30%, and intestinal epithelial permeability (Caco-2) >0 were employed to identify the candidate compounds (19). After this, the target proteins corresponding to the candidate compounds screened from databases were standardized using UniProt (http://www.uniprot.org/) and Genecard (https://www.genecards.org/). Additionally, CRF-related target genes were mined from Malacards (https://www.malacards.org/) or Genecard. The crossover genes were filtered between the 2 lists. The Search Tool for the Retrieval of Interacting Genes/Proteins (STRING) database (https://string-db.org/) was employed to analyze the protein-protein interaction (PPI) network. The JPSSG- compound-CRF-target network was constructed with Cytoscape 3.2.1. The Kyoto Encyclopedia of Genes and Genomes (KEGG) pathway enrichment and Gene Ontology (GO) analysis was carried out with the Database for Annotation, Visualization and Integrated Discovery (DAVID; https://david.ncifcrf.gov/).

Cell culture

The mouse colorectal cancer cell line CT26 and skeletal myoblast cell line C2C12 were obtained from the Cell Bank of the Chinese Academy of Sciences (Shanghai, China). All cells were maintained in Dulbecco's modified Eagle's medium (DMEM; Sigma-Aldrich, St. Louis, MO, USA) supplemented with 10% fetal bovine serum (FBS; Gibco, Thermo Fisher Scientific, Waltham, MA, USA) at 37 ℃ in a 5% CO_2 atmosphere. The C2C12 cells were seeded in 96-well plates (3×10^4 cells/well) or 6-well plates (5×10^5 cells/well) and cultured for 24 h. Afterward, the medium was replaced by DMEM with 2% horse serum (Gibco) for 3 days to induce myotube formation.

Mice

A protocol was prepared before the study without registration. Animal experiments were performed under a project license (No. SPF2017096) approved by the Animal Care and Use Committee of Guangzhou University of Chinese Medicine, in compliance with the institutional guidelines for the care and use of animals. The 6-week-old female Balb/c mice weighing 20–22 g were acquired from SLAC Laboratory Animal Co. (Shanghai, China), and caged at a controlled temperature and humidity and a light-dark cycle. No criteria were set for including or excluding animals. Additionally, no humane end points were established.

Establishment of CRF mouse models and JPSSG treatment

In brief, a total of 12 BALB/c mice were injected with CT26 cells [1×10^6 cells in 0.1 mL of phosphate-buffered saline (PBS)] by intraperitoneal injection and randomly divided into the model group (n=6) and the JPSSG group (n=6). Randomization numbers (1:1:1 random assignment) were generated through the computer and sealed in opaque envelops. The mice in the model group were given oral gavage of PBS, and the mice in the JPSSG group received oral gavage of JPSSG (3 g/kg/day) (the dose was determined by pre-experiment). The prescription of JPSSG was prepared by the pharmacy department of our hospital. The mice in the control group (n=6) were injected with 0.1 mL of PBS by intraperitoneal injection and given oral gavage of the same volume as that of PBS. The oral gavage was performed every day for 15 days. The body weight was measured every 2 days. The behavioral tests were performed before euthanasia according to previous studies (20,21) and included the open field test (OFT), exhaustive swimming test (EST), and tail suspension test (TST). The mice were euthanized, and the peripheral blood, tumor tissues, and gastrocnemius samples were collected. No experimental unit was excluded.

Biochemical index measurements in vivo

The serum was collected from peripheral blood by centrifugation at 2,500 rpm for 20 min. The levels of hemoglobin (Hb), hematocrit (HCT), alanine aminotransferase (ALT), aspartate aminotransferase (AST), total protein (TP), albumin (ALB), globulin (GLOB), creatinine (CR), and blood urea nitrogen (BUN) were detected by hemoglobin analyzer (URIT, China) or fully automatic animal biochemistry analyzer (URIT Medical Electronic Co., Ltd., Guilin, China). The adenosine triphosphate (ATP), superoxide dismutase (SOD), and malondialdehyde (MDA) level in the gastrocnemius samples were detected using reagent kits (Jiancheng Medical Technology Co., Ltd., Jiancheng, China) in accordance with the kits' protocols.

Hematoxylin and eosin staining and electron microscopy

The gastrocnemius samples were fixed using 4%

paraformaldehyde and embedded. Hematoxylin and eosin (HE) staining was performed using an HE Staining Kit (Servicebio Technology Co., Ltd., Wuhan, China). The cross-section areas of myofiber were measured. The gastrocnemius samples were fixed in glutaraldehyde buffer (Solarbio Life Science and Technology, Beijing, China) for 6 h at 4 ℃ and dehydrated through graded alcohol and propylene oxide. The samples were embedded and sliced. The slices were then double-stained using uranyl acetate and lead citrate (HEAD Biotechnology Co., Ltd., Beijing, China) and visualized with an electron microscope (Hitachi, Tokyo, Japan).

Drug sensitivity assay of JPSSG in C2C12 myotubes

The C2C12 myotubes were treated with 0, 2.5, 5, 10, or 20 mg/mL of JPSSG (the concentrations were determined by pre-experiment). After being cultured for 24 h, cell counting kit-8 (CCK-8; Yeasen Biotechnology, Shanghai, China) was adopted to assess cell viability in accordance with the kit's protocol.

JPSSG treatment in C2C12 myotubes

The CT26 cells were plated and cultured for 24 h. The medium was then collected and mixed with fresh medium (1:2) as CT26 conditioned medium (CM). The C2C12 myotubes were stimulated with 100 μM H_2O_2 (Sigma-Aldrich) for 2 h to construct a mitochondrial damage model (22). Briefly, the C2C12 myotubes were divided into 5 groups: a control group (without treatment), a CM group (cultured with CM), a CM + JPSSG group (cultured with CM containing 5 mg/mL of JPSSG), a H_2O_2 group (stimulated with 100 μM of H_2O_2), and a H_2O_2 + JGSSP group (stimulated with 100 μM of H_2O_2 and treated with 5 mg/mL of JPSSG).

Detection of cell viability and cell apoptosis in C2C12 myotubes

The cell viability of C2C12 myotubes at 24 h after treatment were assessed by CCK-8 assay as mentioned above. The cell apoptosis of C2C12 myotubes at 48 h after treatment was assessed with an Annexin V-FITC/PI Kit (Jiancheng Medical Technology Co., Ltd.). In brief, the C2C12 myotubes were collected and resuspended in annexin V (AV) binding buffer. The AV-fluorescein isothiocyanate (AV-FITC) and propidium iodide (PI)

reagent were then added into cell suspension for 20 min at 37 ℃. Flow cytometry analysis was accomplished with a FACSCanto (BD Biosciences, Franklin Lakes, NJ, USA).

Detection of ATP, SOD, MDA, and ROS level in C2C12 myotubes

The ATP, SOD, and MDA level of C2C12 myotubes at 48 h after treatment were detected using reagent kits as mentioned above. The ROS level was assessed using ROS Assay Kit (Beibo Biotechnology, Shanghai, China). Briefly, after 48 h of treatment, the C2C12 myotubes were treated with 10 μM of 2',7'-dichlorodihydrofluorescein diacetate (DCFH-DA) for 30 min at 37 ℃. Cells were then washed with PBS, and the fluorescent images were analyzed using a fluorescence microscope (Olympus, Tokyo, Japan).

Mitochondrial membrane potential in C2C12 myotubes

The mitochondrial membrane potential (MMP) of C2C12 myotubes was determined at 48 h after treatment using an MMP Kit with JC-1 (Jiancheng Medical Technology Co., Ltd.) according to the kit's protocol. The fluorescent images were taken, and the radio of red/green fluorescence intensity was used to measure changes in MMP.

Western blot assay

After 48-h treatment, the total protein of gastrocnemius samples and C2C12 myotubes were isolated by RIPA (Beyotime Biotechnology, Haimen, China). Sodium dodecyl-sulfate polyacrylamide gel electrophoresis (SDS-PAGE) was conducted, and the protein was transferred to polyvinylidene fluoride membranes (BioSharp, Tallinn, Estonia). After being blocked, the membranes were incubated with primary and secondary antibody, successively. Finally, an ECL Kit (Sangon Biotech, Shanghai, China) was used for the detection of protein bands. The antibodies were purchased from Abcam (Cambridge, UK), including p-adenosine 5'-monophosphate-activated protein kinase (AMPK; 1:1,000 and 1:2,000), silent information regulator factor 2-related enzyme 1 (SIRT1) (1:2,000), hypoxia-inducible factor-1α (HIF-1α; 1:500), p-phosphatidylinositol-4,5-bisphosphate 3-kinase (PI3K; 1:2,000 and 1:1,000), p-protein kinase B (AKT; 1:2,000 and 1:1,000), cleaved caspase-3 (C-caspase 3) (1:1,000), B-cell lymphoma-2 (Bcl2, 1:1,000), GAPDH (1:5,000), and goat anti-rabbit immunoglobin G (IgG; H + L) horseradish peroxidase

antibody (1:10,000).

Statistical analysis

GraphPad Prism 8.0 software (GraphPad Software Inc., San Diego, CA, USA) was used for all statistical analysis in this study. The weight of tumor was analyzed using unpaired Student t-test. One-way analysis of variance (ANOVA) with Dunnett or Tukey multiple comparisons test was used for other analyses. $P<0.05$ was considered as statistically significant.

Results

Network pharmacology analysis of JPSSG

A total of 617 active compounds of JPSSG were obtained through searching the TCMSP; http://lsp.nwu.edu.cn/index.php). Following this, 87 candidate bioactive compounds that met the conditions (DL ≥ 0.18, OB $\geq 30\%$, and Caco-2 >0) were finally identified for further analysis; their detailed information is listed in *Table 1*.

Among the aforementioned 87 bioactive compounds of JPSSG, 248 potential targets were identified. After removal of the duplicate data and standardized processing, 132 CRF-related JPSSG targets were subsequently obtained, which were then used to construct the PPI network diagram (*Figure 1A*) and the corresponding hub diagram (*Figure 1B*) using STRING database analysis. Furthermore, the JPSSG-CRF interaction targets were analyzed through the PPI network via Cytoscape 3.2.1 software (*Figure 1C*). The network included 198 nodes and 412 edges, which indicated that JPSSG treated CRF through multicomponent,

Table 1 Bioactive compounds of JPSSG

Mol ID	Molecule name	OB (%)	DL
MOL005030	Gondoic acid	30.7	0.2
MOL006944	8-octadecenoic acid	33.13	0.14
MOL000359	Sitosterol	36.91	0.75
MOL004328	Naringenin	59.29	0.21
MOL005100	5,7-dihydroxy-2-(3-hydroxy-4-methoxyphenyl) chroman-4-one	47.74	0.27
MOL005815	Citromitin	86.9	0.51
MOL005828	Nobiletin	61.67	0.52
MOL000006	Luteolin	36.16	0.25
MOL000449	Stigmasterol	43.83	0.76
MOL001006	Poriferasta-7,22E-dien-3beta-ol	42.98	0.76
MOL002140	Perlolyrine	65.95	0.27
MOL002879	Diop	43.59	0.39
MOL003036	Zinc03978781	43.83	0.76
MOL003896	7-Methoxy-2-methyl isoflavone	42.56	0.2
MOL004355	Spinasterol	42.98	0.76
MOL004492	Chrysanthemaxanthin	38.72	0.58
MOL005321	Frutinone A	65.9	0.34
MOL006554	Taraxerol	38.4	0.77
MOL006774	Stigmasta-7-enol	37.42	0.75
MOL007059	3-beta-Hydroxymethyllenetanshiquinone	32.16	0.41

Table 1 (*continued*)

Table 1 (*continued*)

Mol ID	Molecule name	OB (%)	DL
MOL007514	Methyl icosa-11,14-dienoate	39.67	0.23
MOL008391	5alpha-Stigmastan-3,6-dione	33.12	0.79
MOL008397	Daturilin	50.37	0.77
MOL008400	Glycitein	50.48	0.24
MOL008407	(8S,9S,10R,13R,14S,17R)-17-[(E,2R,5S)-5-ethyl-6-methylhept-3-en-2-yl]-10,13-dimethyl-1,2,4,7,8,9,11,12,14,15,16,17-dodecahydrocyclopenta[a]phenanthren-3-one	45.4	0.76
MOL008411	11-hydroxyrankinidine	40	0.66
MOL000098	Quercetin	46.43	0.28
MOL000358	Beta-sitosterol	36.91	0.75
MOL000953	Clr	37.87	0.68
MOL001323	Sitosterol alpha1	43.28	0.78
MOL001494	Mandenol	42	0.19
MOL001495	Ethyl linolenate	46.1	0.2
MOL001979	Lan	42.12	0.75
MOL003578	Cycloartenol	38.69	0.78
MOL005406	Atropine	45.97	0.19
MOL005438	Campesterol	37.58	0.71
MOL006209	Cyanin	47.42	0.76
MOL007449	24-methylidenelophenol	44.19	0.75
MOL008173	Daucosterol_qt	36.91	0.75
MOL009604	14b-pregnane	34.78	0.34
MOL009612	(24R)-4alpha-Methyl-24-ethylcholesta-7,25-dien-3beta-ylacetate	46.36	0.84
MOL009615	24-Methylenecycloartan-3beta,21-diol	37.32	0.8
MOL009617	24-ethylcholest-22-enol	37.09	0.75
MOL009618	24-ethylcholesta-5,22-dienol	43.83	0.76
MOL009620	24-methyl-31-norlanost-9(11)-enol	38	0.75
MOL009621	24-methylenelanost-8-enol	42.37	0.77
MOL009622	Fucosterol	43.78	0.76
MOL009631	31-norcyclolaudenol	38.68	0.81
MOL009633	31-norlanost-9(11)-enol	38.35	0.72
MOL009634	31-norlanosterol	42.2	0.73
MOL009635	4,24-methyllophenol	37.83	0.75
MOL009639	Lophenol	38.13	0.71
MOL009640	4alpha,14alpha,24-trimethylcholesta-8,24-dienol	38.91	0.76

Table 1 (*continued*)

Table 1 (*continued*)

Mol ID	Molecule name	OB (%)	DL
MOL009641	4alpha,24-dimethylcholesta-7,24-dienol	42.65	0.75
MOL009642	4alpha-methyl-24-ethylcholesta-7,24-dienol	42.3	0.78
MOL009644	6-fluoroindole-7-dehydrocholesterol	43.73	0.72
MOL009646	7-O-Methylluteolin-6-C-beta-glucoside_qt	40.77	0.3
MOL009650	Atropine	42.16	0.19
MOL009651	Cryptoxanthin monoepoxide	46.95	0.56
MOL009653	Cycloeucalenol	39.73	0.79
MOL009656	(E,E)-1-ethyl octadeca-3,13-dienoate	42	0.19
MOL009662	Lantadene A	38.68	0.57
MOL009677	Lanost-8-en-3beta-ol	34.23	0.74
MOL009678	Lanost-8-enol	34.23	0.74
MOL009681	Obtusifoliol	42.55	0.76
MOL010234	Delta-Carotene	31.8	0.55
MOL000546	Diosgenin	80.88	0.81
MOL001792	Dfv	32.76	0.18
MOL002714	Baicalein	33.52	0.21
MOL002959	3'-methoxydaidzein	48.57	0.24
MOL003889	Methylprotodioscin_qt	35.12	0.86
MOL004941	(2R)-7-hydroxy-2-(4-hydroxyphenyl)chroman-4-one	71.12	0.18
MOL006331	4',5-dihydroxyflavone	48.55	0.19
MOL009760	Sibiricoside A_qt	35.26	0.86
MOL009766	Zhonghualiaoine 1	34.72	0.78
MOL001689	Acacetin	34.97	0.24
MOL002975	Butin	69.94	0.21
MOL003378	1,3,8,9-tetrahydroxybenzofurano[3,2-c]chromen-6-one	33.94	0.43
MOL003389	3'-o-methylorobol	57.41	0.27
MOL003398	Pratensein	39.06	0.28
MOL003402	Demethylwedelolactone	72.13	0.43
MOL003404	Wedelolactone	49.6	0.48
MOL000422	Kaempferol	41.88	0.24
MOL005169	(20S)-24-ene-3,20-diol-3-acetate	40.23	0.82
MOL005190	Eriodictyol	71.79	0.24
MOL005195	Syringaresinol diglucoside_qt	83.12	0.8
MOL005209	Lucidusculine	30.11	0.75

JPSSG, Jian Pi Sheng Sui Gao; OB, oral bioavailability; DL, drug likeness.
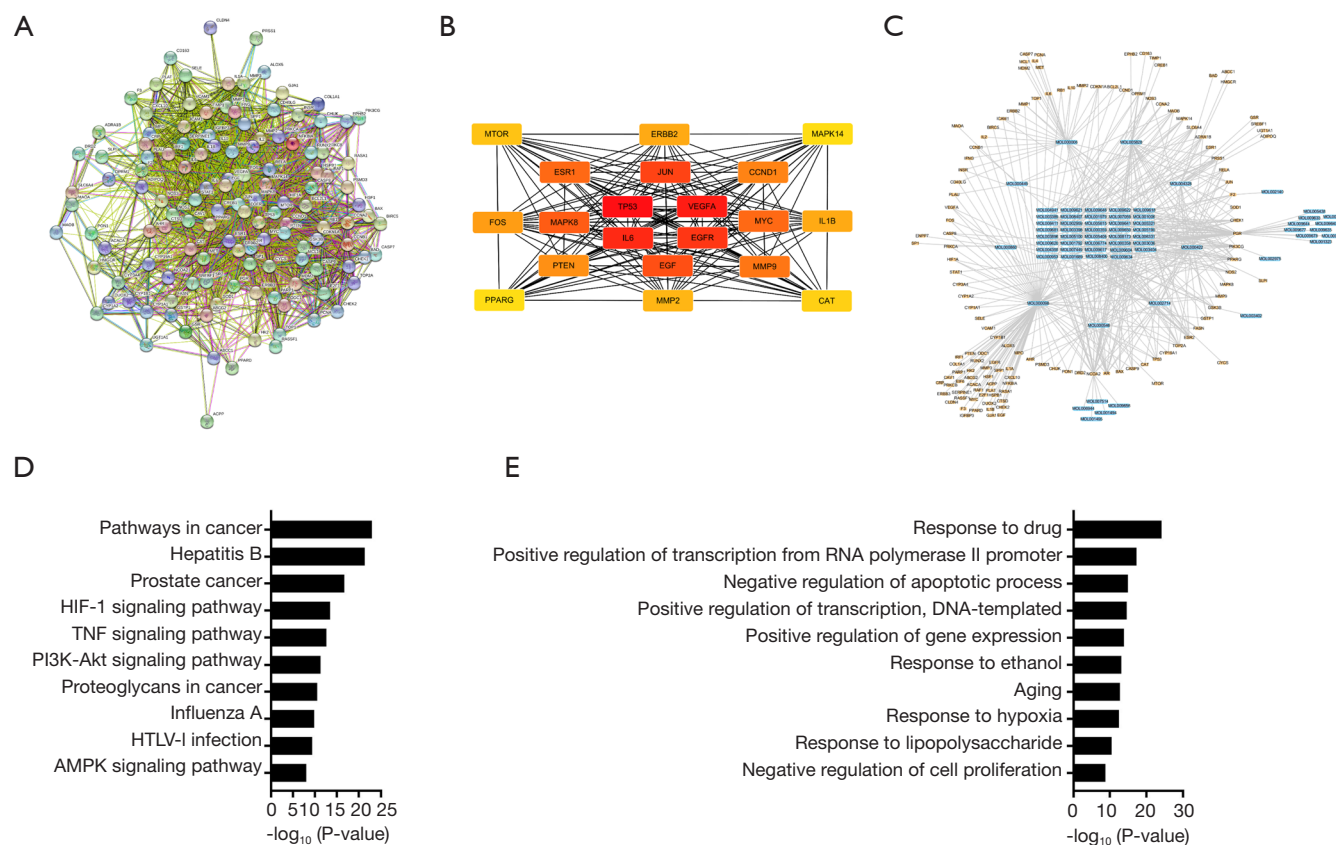
Figure 1 The potential targets, pathways, and biological processes of the JPSSG-CRF interaction. The PPI network diagram of JPSSG targets that were related to CRF (A) and its hub diagram (B). The PPI network diagram of JPSSG-CRF interaction targets; the blue rectangles represent the compounds and the yellow rectangles represent the target genes (C). The underlying pathways obtained from the KEGG enrichment analysis (D). The underlying biological processes obtained from the GO enrichment analysis (E). JPSSG, Jian Pi Sheng Sui Gao; CRF, cancer-related fatigue; PPI, protein-protein interaction; KEGG, Kyoto Encyclopedia of Genes and Genomes; GO, Gene Ontology; HIF-1, hypoxia-inducible factor-1; TNF, tumor necrosis factor; PI3K-Akt, phosphatidylinositol-4,5-bisphosphate 3-kinase-protein kinase B; HTLV-I, human T-lymphotropic virus type 1; IL, interleukin; MTOR, mammalian target of rapamycin; EGFR, epidermal growth factor receptor; MMP, matrix metalloproteinase; VEGFA, vascular endothelial growth factor A.

multitarget, and integrated regulation.

Based on the KEGG enrichment analysis, 10 underlying pathways were obtained (conforming to P≤0.01 and gene frequency >0.09%), including pathways in cancer, hepatitis B, prostate cancer, HIF-1 signaling pathway, tumor necrosis factor (TNF) signaling pathway, PI3K-AKT signaling pathway, proteoglycans in cancer, influenza A, human T-lymphotropic virus type 1 (HTLV-I) infection, and AMPK signaling pathway (*Figure 1D*). Moreover, the GO enrichment analysis was also performed, and 10 biological processes were found to be enriched (conforming to P≤0.01 and gene frequency >0.065%), including response to drug, positive regulation of transcription from RNA

polymerase II promoter, negative regulation of apoptotic process, positive regulation of transcription, DNA template, positive regulation of gene expression, response to ethanol, aging, response to hypoxia, response to lipopolysaccharide, and negative regulation of cell proliferation (*Figure 1E*). Based on the above analysis results, AMPK-SIRT1, HIF-1, and PI3K-AKT were selected as the potential signaling pathways mediated by JPSSG for the subsequent *in vivo* and *in vitro* studies.

Influence of JPSSG on fatigue in CRF mouse models

The OFT revealed that distance traveled (P<0.001;
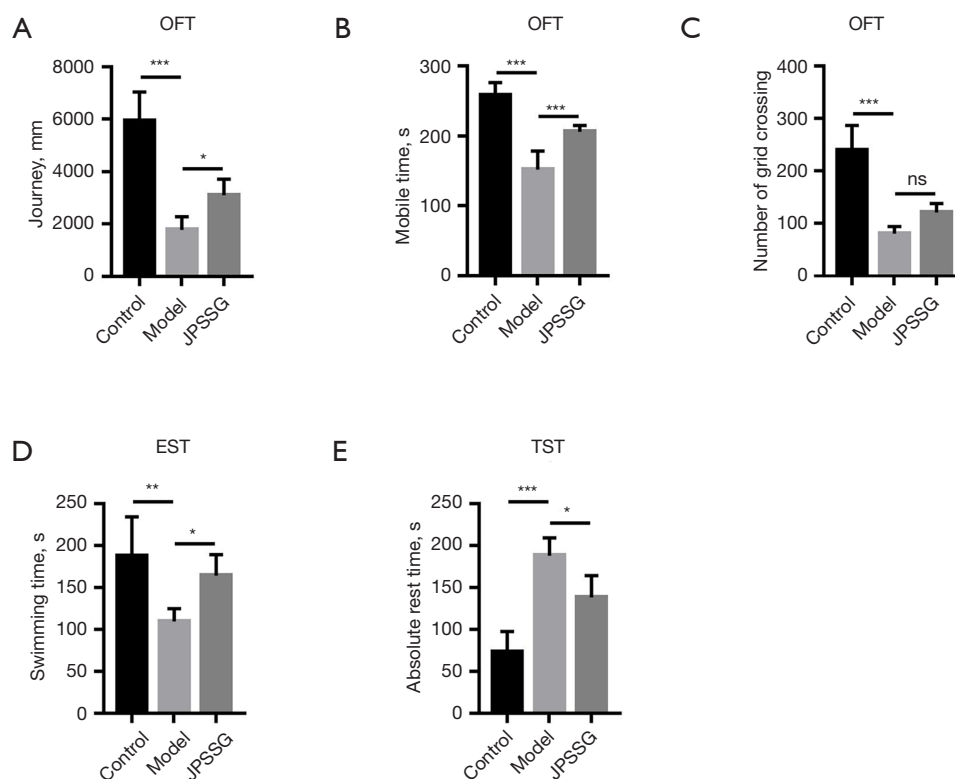
Figure 2 JPSSG ameliorated fatigue in the CRF mouse models. Influence of JPSSG on distance traveled (A), mobile time (B), number of grid crossing (C), swimming time (D), and absolute rest time (E) in the CRF mouse models. ***, P<0.001; **, P<0.010; *, P<0.050; ns, nonsignificant. JPSSG, Jian Pi Sheng Sui Gao; CRF, cancer-related fatigue; OFT, open field test; EST, exhaustive swimming test; TST, tail suspension test.

Figure 2A), mobile time (P<0.001, *Figure 2B*), and number of grid crossings (P<0.001; *Figure 2C*) were all decreased in the model group compared to the control group, indicating the successful establishment of the CRF mouse models. Meanwhile, distance traveled (P<0.050; *Figure 2A*) and mobile time (P<0.001; *Figure 2B*) were both increased in the JPSSG group compared to the model group, but the number of grid crossings was not different between the JPSSG group and the model group (P>0.050; *Figure 2C*). For the EST, the swimming time was reduced in the model group compared to control group (P<0.010) but was elevated in the JPSSG group compared to the model group (P<0.050; *Figure 2D*). For the TST, the absolute rest time was prolonged in the model group (*vs.* control group; P<0.001) and shortened in the JPSSG group (*vs.* model group; P<0.050; *Figure 2E*). These findings showed that JPSSG could alleviate CRF to some extent.

Influence of JPSSG on the weight and blood biochemical indices of the CRF mouse models

The body-weight curves suggested that the body weights of mice in the control group, model group, and JPSSG group all slightly fluctuated within 15 days after injection (*Figure 3A*). Specifically, on day 7, 9, 11, 13, and 15, the body weights of mice in JPSSG group showed a decreasing trend (without statistical significance) than did those in the model group. The tumor weight was not different between the JPSSG group and model group (P>0.050; *Figure 3B*), whereas, the gastrocnemius weight was reduced in the model group (*vs.* control group; P<0.001) but was elevated in the JPSSG group (*vs.* model group; P<0.050; *Figure 3C*), indicating that JPSSG could ameliorate the myophagism of gastrocnemius.

Hb (P<0.001; *Figure 3D*) and HCT (P<0.001;
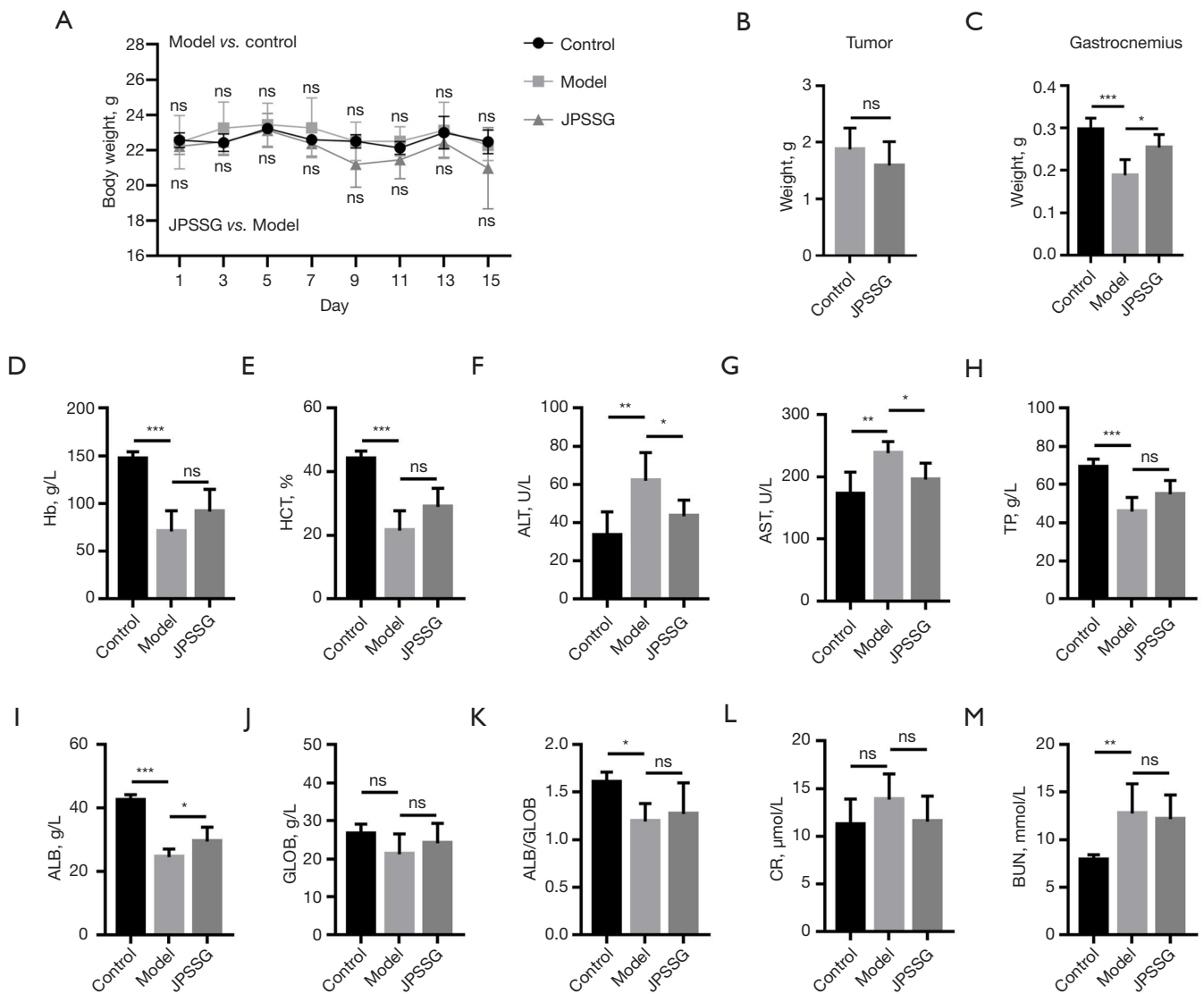
Figure 3 JPSSG alleviated gastrocnemius weight reduction and hepatic function impairment in CRF mouse models. Influence of JPSSG on body weight (A), tumor weight (B), gastrocnemius weight (C), Hb (D), HCT (E), ALT (F), AST (G), TP (H), ALB (I), GLOB (J). ALB/GLOB (K), CR (L), and BUN (M) in the CRF mouse models. ***, P<0.001; **, P<0.010; *, P<0.050; ns, nonsignificant. JPSSG, Jian Pi Sheng Sui Gao; CRF, cancer-related fatigue; Hb, hemoglobin; HCT, hematocrit; ALT, alanine aminotransferase; AST, aspartate aminotransferase; TP, total protein; ALB, albumin; GLOB, globulin; CR, creatinine; BUN, blood urea nitrogen.

Figure 3E) were reduced in the model group compared to the control group, but they showed an increasing trend (lacking statistical significance) in the JPSSG group compared with model group (both P>0.050), indicating that JPSSG had the potency to suppress cancer-induced anemia. ALT (P<0.010; *Figure 3F*) and AST (P<0.010; *Figure 3G*) were increased in the model group compared to the control group but were decreased in the JPSSG group compared

to the model group (both P values <0.050). TP (P<0.001), ALB (P<0.001), and ALB/GLOB (P<0.050) were decreased in the model group (*vs.* control group), while GLOB (P>0.050) showed no difference between these 2 groups (*Figure 3H-3K*). Only ALB was upregulated in the JPSSG group compared with the model group (P<0.050), while TP, GLOB, and ALB/GLOB were not different between these 2 groups (all P>0.050). Additionally, CR showed an increasing

trend (without statistical significance) in the model group (*vs.* control group; P>0.050), and BUN was higher in the model group than in the control group (P<0.010); nonetheless, CR and BUN levels showed no difference between the JPSSG group and model group (both P>0.050; *Figure 3L,3M*). The results suggest that JPSSG can improve hepatic function impairment, while its effect on relieving renal injury was relatively weak.

Influence of JPSSG on oxidative stress and mitochondrial function in CRF mouse models

ATP (P<0.010, *Figure 4A*) and SOD (P<0.010, *Figure 4B*) were reduced while MDA (P<0.010, *Figure 4C*) was elevated in the model group (*vs.* control group); ATP and SOD were upregulated in the JPSSG group (*vs.* model group; both P<0.050), whereas MDA was not different between these 2 groups (P>0.050), indicating that JPSSG could enhance mitochondrial function and alleviate oxidative stress in gastrocnemius. Moreover, the cross-sectional area of the gastrocnemius was decreased in the model group compared with the control group (P<0.001) but was increased in the JPSSG group compared to the model group (P<0.050; *Figure 4D*). Moreover, the HE staining of the gastrocnemius samples suggested that JPSSG could suppress the damage to skeletal muscle cells (*Figure 4E*). Additionally, the electron microscopy results of gastrocnemius mitochondria revealed that the shape and number of mitochondria were partially improved by JPSSG (*Figure 4F*).

Determination of JPSSG-mediated pathways in CRF mouse models

The AMPK-SIRT1, HIF-1, and PI3K-AKT signaling pathway-related proteins were determined by Western blot (*Figure 5A*). p-AMPK (P<0.010; *Figure 5B*) and SIRT1 (P<0.010; *Figure 5C*) were both decreased in the model group (*vs.* control group) while they were elevated in the JPSSG group (*vs.* model group; both P<0.050); HIF-1α was not different between the model group and control group (P>0.050) but was elevated in the JPSSG group (*vs.* model group; P<0.010; *Figure 5D*); p-PI3K (P<0.050, *Figure 5E*) and p-AKT (P<0.050; *Figure 5F*) were downregulated in the model group (*vs.* control group), but they were not different between the JPSSG group and the model group (both P>0.050), suggesting that AMPK-SIRT1 and HIF-1 might be the main signaling pathways regulated by JPSSG.

Influence of JPSSG on cell viability and cell apoptosis in C2C12 myotubes

C2C12 cell viability was not different under different JPSSG concentrations (0, 2.5, 5, 10, and 20 mg/mL; all P>0.050, *Figure 6A*). C2C12 cell viability was decreased in the CM group and H_2O_2 group (*vs.* control group) (both P<0.001) while it was elevated in the CM + JPSSG group (*vs.* CM group) and H_2O_2 + JPSSG group (*vs.* H_2O_2 group; both P<0.050; *Figure 6B*). With regard to cell apoptosis, the apoptosis rate was increased in the CM group and H_2O_2 group (*vs.* control group; both P<0.001); meanwhile, it was reduced in the CM + JPSSG group (*vs.* CM group; P<0.050) and H_2O_2 + JPSSG group (*vs.* H_2O_2 group; P<0.010; *Figure 6C,6D*). According to Western blot (*Figure 6E*), C-caspase3 was elevated in the CM group (P<0.010) and H_2O_2 group (P<0.001; *vs.* control group) but was decreased in the CM + JPSSG group (*vs.* CM group; P<0.050) and H_2O_2 + JPSSG group (*vs.* H_2O_2 group; P<0.010; *Figure 6F*). However, Bcl2 was decreased in the CM group and H_2O_2 group (*vs.* control group; both P<0.001), while it was upregulated in the CM + JPSSG group (*vs.* CM group) and H_2O_2 + JPSSG group (*vs.* H_2O_2 group; both P<0.050; *Figure 6G*). The results indicate that JPSSG facilitated cell viability and suppressed cell apoptosis in C2C12 myotubes.

Influence of JPSSG on oxidative stress and mitochondrial function in C2C12 myotubes

ATP was reduced in the CM group (P<0.010) and H_2O_2 group (P<0.001; *vs.* control group) but was elevated in the CM + JPSSG group (*vs.* CM group) and H_2O_2 + JPSSG group (*vs.* H_2O_2 group; both P<0.050; *Figure 7A*), suggesting that JPSSG could enhance mitochondrial function in C2C12 cells. SOD was downregulated in the CM group and H_2O_2 group (*vs.* control group; both P<0.001) but it was upregulated in the CM + JPSSG group (*vs.* CM group) and H_2O_2 + JPSSG group (*vs.* H_2O_2 group; both P<0.050; *Figure 7B*). Conversely, MDA (*Figure 7C*) and the relative ROS level (*Figure 7D,7E*) were increased in the CM group (*vs.* control group; MDA: P<0.010; ROS: P<0.001) and H_2O_2 group (*vs.* control group; both P<0.001), while they were decreased in the CM + JPSSG group (*vs.* CM group) and H_2O_2 + JPSSG group (*vs.* H_2O_2 group; all P<0.050), indicating that JPSSG could restrain oxidative stress levels of gastrocnemius. MMP, as reflected by the red:green fluorescence ratio, was downregulated in
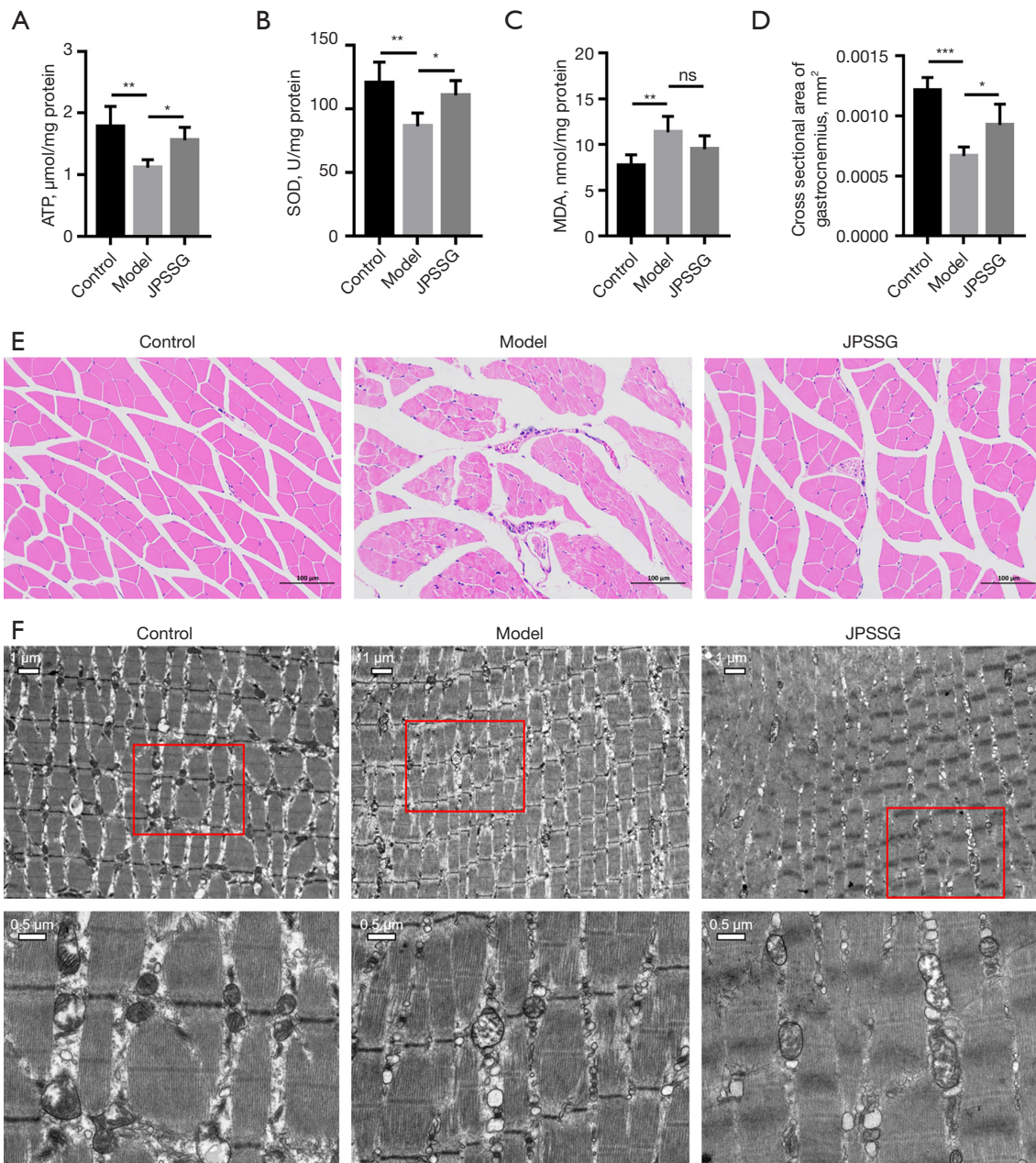
Figure 4 JPSSG suppressed oxidative stress and mitochondria damage in the CRF mouse models. Influence of JPSSG on ATP (A), SOD (B), MDA (C), and the cross-sectional area of the gastrocnemius (D) in the CRF mouse models. The HE staining of gastrocnemius samples (E). The electron microscopy examples of the gastrocnemius mitochondria (F). ***, $P<0.001$; **, $P<0.010$; *, $P<0.050$; ns, nonsignificant. JPSSG, Jian Pi Sheng Sui Gao; CRF, cancer-related fatigue; ATP, adenosine triphosphate; SOD, superoxide dismutase; MDA, malondialdehyde; HE, hematoxylin and eosin.

the CM group and H_2O_2 group (*vs.* control group; both $P<0.001$) and was upregulated in the CM + JPSSG group (*vs.* CM group; $P<0.010$) and H_2O_2 + JPSSG group (*vs.* H_2O_2 group; $P<0.050$; *Figure 7F,7G*), implying that JPSSG could suppress the reduction of MMP in cell myotubes.

Determination of JPSSG-mediated pathways in C2C12 myotubes

According to Western blot, (*Figure 8A*), p-AMPK was reduced in the CM group ($P<0.010$) and H_2O_2 group
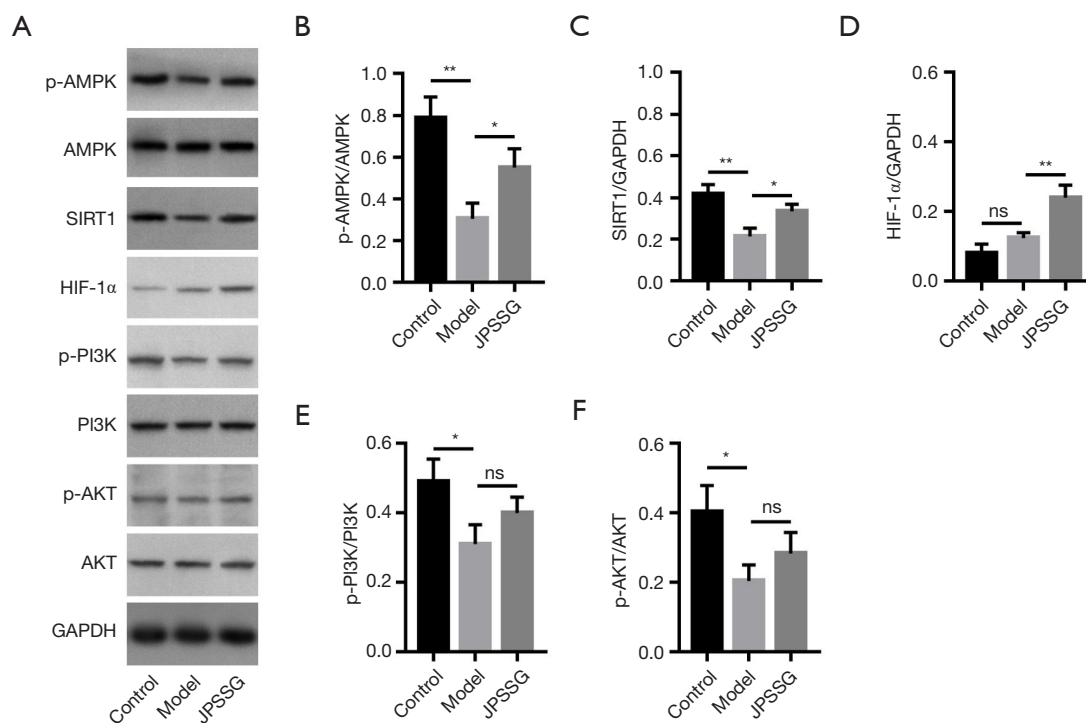
Figure 5 JPSSG activated the AMPK-SIRT1 pathway and HIF-1 pathway in the CRF mouse models. Presentation of Western blot bands (A) and further comparison of p-AMPK (B), SIRT1 (C), HIF-1α (D), p-PI3K (E), and p-AKT (F) among the control, model, and JPSSG groups in the CRF mouse models. **, $P < 0.010$; *, $P < 0.050$; ns, nonsignificant. JPSSG, Jian Pi Sheng Sui Gao; CRF, cancer-related fatigue; AMPK, adenosine 5'-monophosphate-activated protein kinase; SIRT1, silent information regulator factor 2-related enzyme 1; HIF-1α, hypoxia-inducible factor-1α; PI3K, phosphatidylinositol-4,5-bisphosphate 3-kinase; AKT, protein kinase B.

($P < 0.001$; *vs.* control group) but was elevated in the CM+JPSSG group (*vs.* CM group) and H_2O_2 + JPSSG group (*vs.* H_2O_2 group; both P values <0.050; *Figure 8B*). Similarly, SIRT1 was downregulated in the CM group ($P < 0.050$) and H_2O_2 group ($P < 0.010$; *vs.* control group) but was upregulated in the H_2O_2 + JPSSG group (*vs.* H_2O_2 group; $P < 0.050$), with no difference being found between the CM + JPSSG group and CM group ($P > 0.050$; *Figure 8C*). Furthermore, HIF-1α was not different between the CM group and control group ($P > 0.050$) but was elevated in the H_2O_2 group (*vs.* control group; $P < 0.010$); meanwhile, HIF-1α was elevated in the CM + JPSSG group (*vs.* CM group) and H_2O_2 + JPSSG group (*vs.* H_2O_2 group; both $P < 0.010$; *Figure 8D*), indicating that JPSSG could bolster the antioxidative stress function via regulating the AMPK-SIRT1 and HIF-1 pathways.

Discussion

As JPSSG comprises 17 different kinds of herbs, its

underlying biological mechanism is complex. Through network pharmacology analysis, this study found that JPSSG contained a total of 87 potential active compounds (mainly including citromitin, nobiletin, frutinone A, daturilin, diosgenin, demethylwedelolactone, syringaresinol-diglucoside), 132 JPSSG-CRF interaction targets, 10 potential pathways (mainly including PI3K-AKT, HIF-1, and AMPK signaling pathways), and 19 biological processes (mainly including hypoxia response, lipopolysaccharide response, negative cell proliferation). These findings clarify the JPSSG-CRF interaction network and provide reliable evidence for subsequent *in vivo* and *in vitro* experiments.

The current study observed that JPSSG attenuated CRF in mice reflected by increased distance traveled, mobile time, swimming time, and decreased absolute rest time in the JPSSG group (*vs.* model group), which revealed the potential treatment efficacy of JPSSG in those with CRF. These findings might be explained as follows: (I) as disclosed in our *in vitro* experiment, JPSSG promoted cell
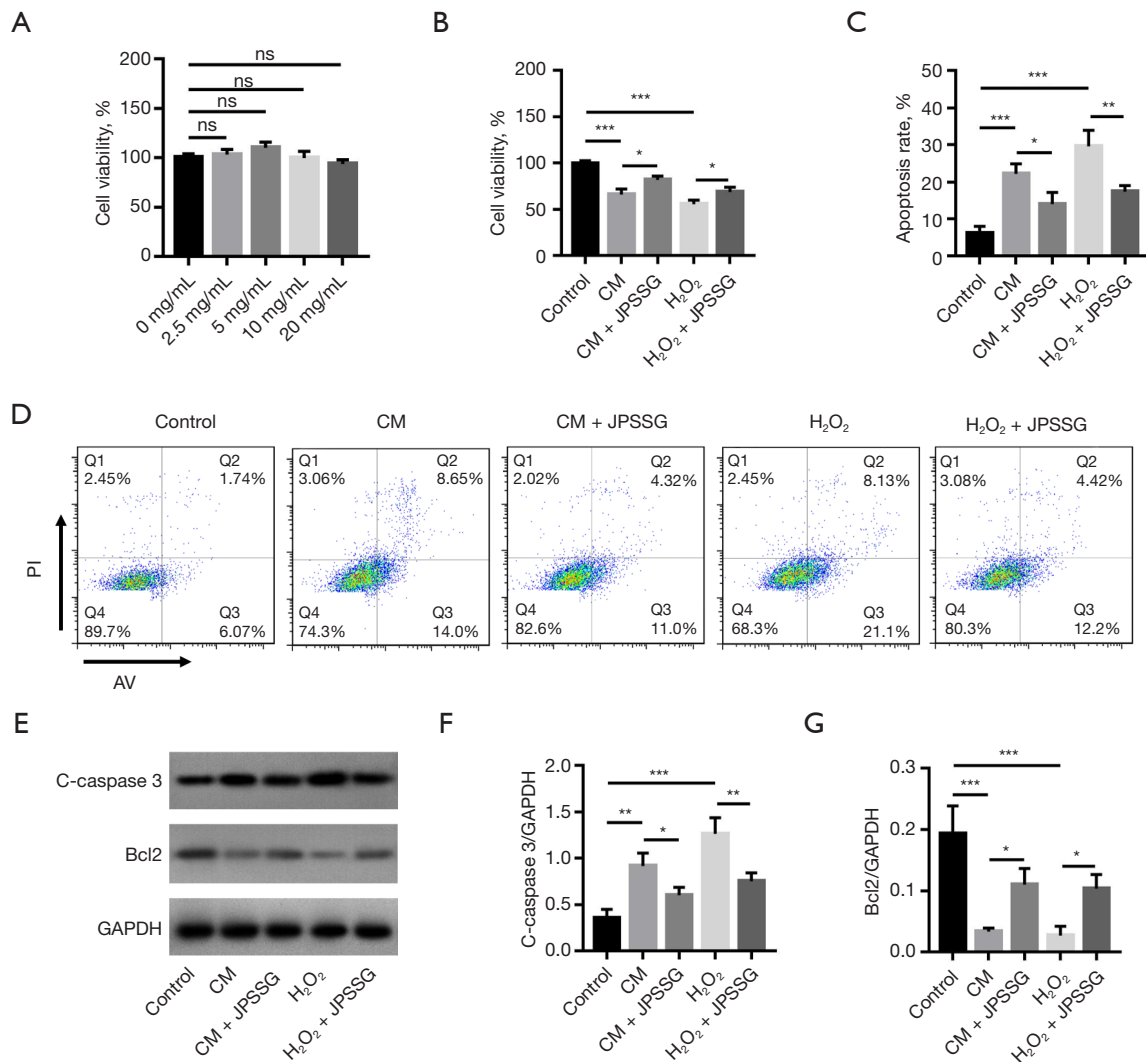
Figure 6 JPSSG enhanced cell viability and restrained cell apoptosis in the C2C12 myotubes. Comparison of C2C12 cell viability under different JPSSG concentrations (A). Influence of JPSSG on cell viability (B) and apoptosis rate (C). An AV-PI staining example reflecting the influence of JPSSG on cell apoptosis (D). Examples of Western blot displaying the effect of JPSSG on C-caspase 3 and Bcl2 (E). Influence of JPSSG on C-caspase 3 (F) and Bcl2 (G). ***, $P<0.001$; **, $P<0.010$; *, $P<0.050$; ns, nonsignificant. JPSSG, Jian Pi Sheng Sui Gao; AV, annexin V; PI, propidium iodide; CM, conditioned medium; C-caspase 3, cleaved caspase-3; Bcl2, B-cell lymphoma-2.

viability and reduced cell apoptosis of gastrocnemius cells; thus, the musculoskeletal function was improved (23). (II) The steroidal components (such as daturilin and diosgenin) of JPSSG ameliorated the inflammatory response and circadian rhythm dysfunction, while the latter 2 factors (inflammatory response and circadian rhythm dysfunction) participated in the deterioration of CRF (24-26). (III) Based on the network pharmacological analysis results, JPSSG mediated the AMPK-SIRT1 and HIF-1 signaling pathways, which protected the gastrocnemius from hypoxia injury and

further induced fatigue resistance (27,28). Combining the above reasons, we can see that JPSSG reduced the fatigue behavioral phenotype in CRF mouse models.

Oxidative stress represents the imbalance between ROS and the antioxidant system and can lead to further molecular damage (29,30). Some previous studies have noted that oxidative stress is a key contributor to the formation and progression of cancer and that a high level of oxidants can cause muscle weakness and further aggravate fatigue degree (31-34). This study found that JPSSG suppressed oxidative
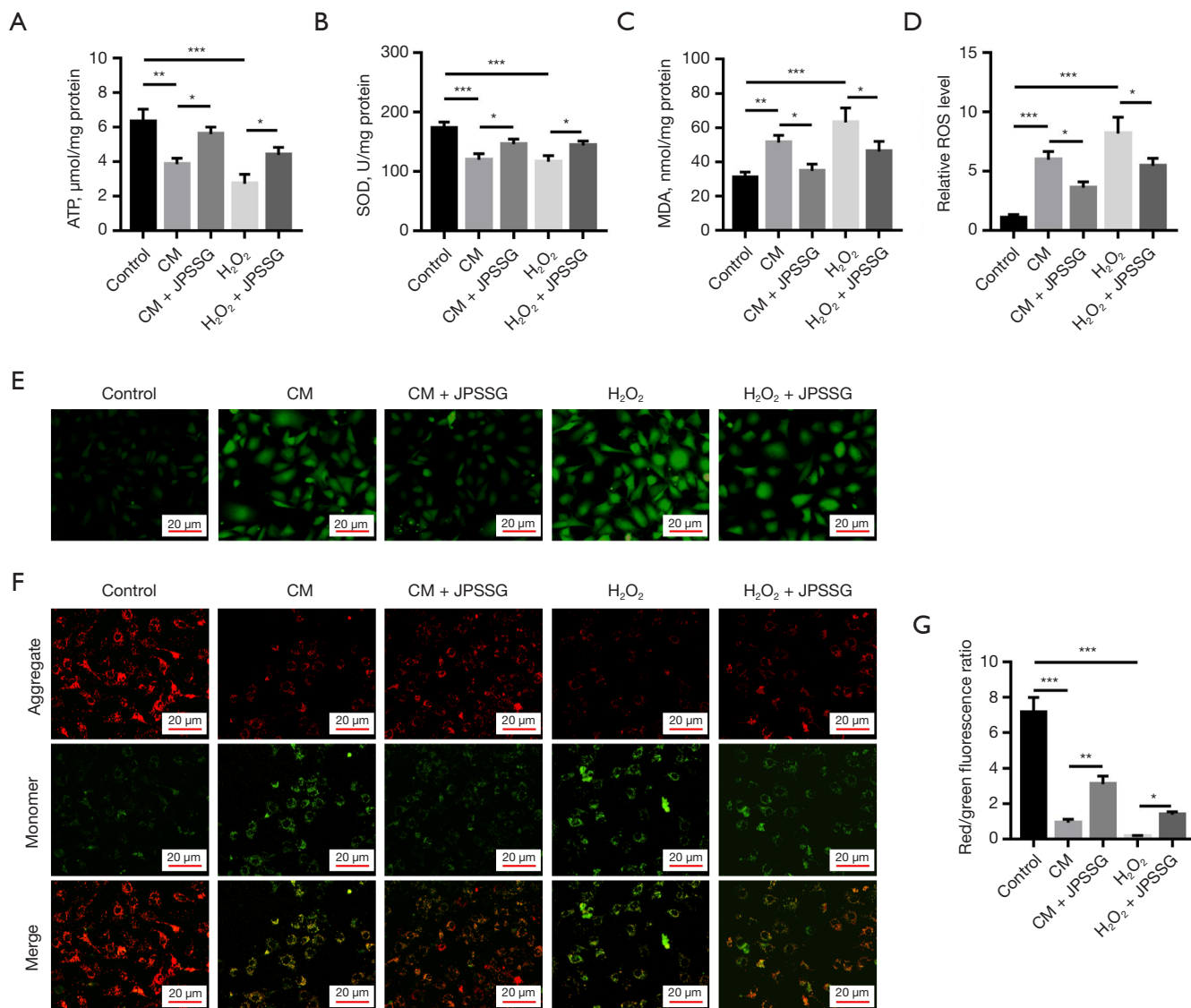
Figure 7 PSSG restrained oxidative stress and mitochondrial damage in C2C12 myotubes. Influence of JPSSG on ATP (A), SOD (B), and MDA (C). Effect of JPSSG on relative ROS level (D) and the corresponding fluorescent images (E). The related fluorescent images (F) and the influence of JPSSG on MMP (G). ***, P<0.001; **, P<0.010; *, P<0.050. JPSSG, Jian Pi Sheng Sui Gao; ATP, adenosine triphosphate; SOD, superoxide dismutase; MDA, malondialdehyde; ROS, reactive oxygen species; CM, conditioned medium.

stress and mitochondrial injury in both CRF mouse models and C2C12 myotubes through upregulating ATP and SOD but downregulating MDA, which is the same mechanism present in patients with CRF. Possible explanations for this might be the following: (I) coumarin components (such as frutinone A and demethylwedelolactone) in JPSSG could limit the oxidative stress response and hypoxia injury via regulating matrix metalloproteinases (35,36). Consequently, JPSSG could suppress oxidative stress in CRF mouse models and C2C12 myotubes. (II) The

bioactive components of JPSSG could inactivate CYP1A1 and CYP1A2, thus ameliorating oxidative stress and mitochondrial injury (37,38). Therefore, JPSSG inhibited oxidative stress and mitochondrial dysfunction in CRF mouse models and C2C12 myotubes.

AMPK-SIRT1, which is regarded as the control node of mitochondria, is a key signaling pathway that regulates the whole-body energy metabolism (including lipid, glucose metabolism, and other biological processes) via binding to adenine nucleotides (27,39). A previous study reported
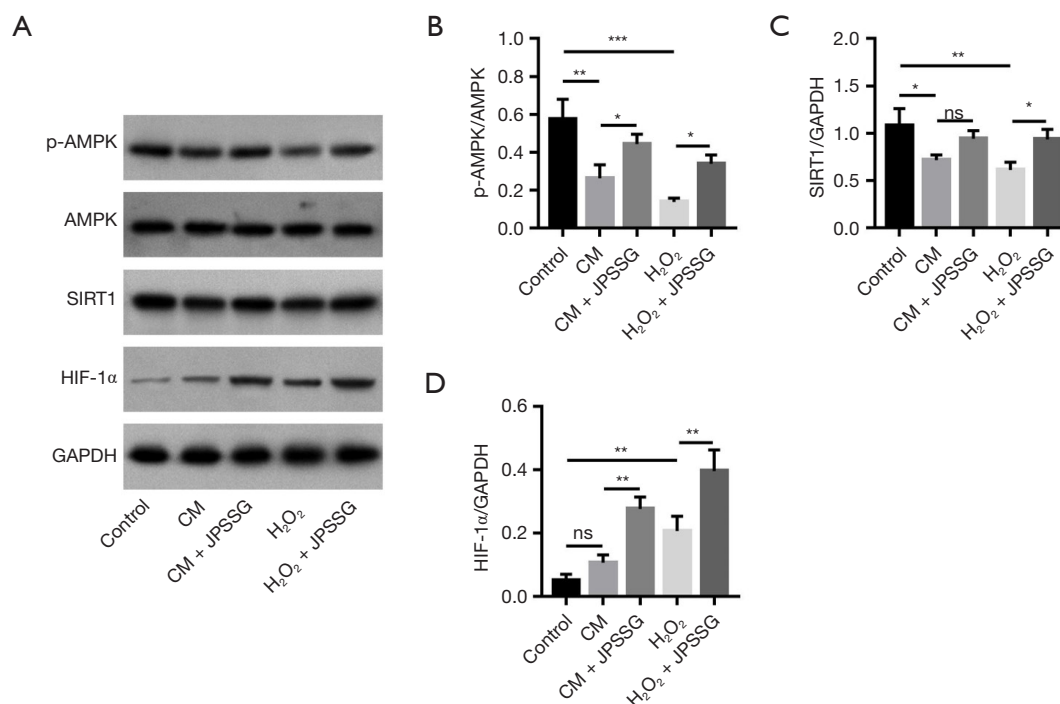
Figure 8 JPSSG promoted AMPK-SIRT1 pathway and HIF-1 pathway in C2C12 myotubes. Presentation of Western blot bands (A) and further comparison of p-AMPK (B), SIRT1 (C), and HIF-1α (D) among the groups in C2C12 myotubes. ***, $P<0.001$; **, $P<0.010$; *, $P<0.050$; ns, nonsignificant. JPSSG, Jian Pi Sheng Sui Gao; AMPK, adenosine 5'-monophosphate-activated protein kinase; SIRT1, silent information regulator factor 2-related enzyme 1; HIF-1α, hypoxia-inducible factor-1α; CM, conditioned medium.

that the AMPK-SIRT1 pathway is involved in the acute metabolic response of skeletal muscles via increasing the number of mitochondria (40). As for the HIF-1 signaling pathway, it is a major regulator in maintaining oxygen homeostasis in a hypoxic environment by regulating ROS level (41). One study reported that the activation of HIF-1 signaling pathway could reduce the susceptibility of muscles to oxidative stress (28). In view of these previous findings, we speculated that AMPK-SIRT1 and HIF-1 pathways might be implicated in the effect of JPSSG on CRF, but the relevant evidence was limited. In this study, JPSSG was shown to activate AMPK-SIRT1 and HIF-1 signaling pathways, and this might be the underlying mechanism for the ameliorating effect of JPSSG on CRF.

Some limitations of this study should be noted. Firs, the correlation of the core active compounds of JPSSG with the potential pathways (such as AMPK-SIRT1 and HIF-1 signaling pathways) was not examined in this study, and thus further research is warranted. Second, the relatively small sample size (N=18) inevitably weakened the statistical power. Third, CRF is induced by both the cancer itself and cancer-related treatment, but the current study did not include a cancer-related treatment intervention; therefore, the effect of JPSSG on cancer-related treatment-induced CRF should be examined in future research. Fourth, this study only set one JPSSG dose, and the comparison of effect on CRF between high and low dose JPSSG should be investigated in further studies.

Conclusions

Collectively, JPSSG alleviates CRF via improving skeletal myoblast cell apoptosis, oxidative stress, and mitochondrial dysfunction in an AMPK-SIRT1- and HIF-1-dependent manner.

Acknowledgments

Footnote

amegroups.com/article/view/10.21037/atm-22-6611/rc

Data Sharing Statement: Available at https://atm.amegroups.com/article/view/10.21037/atm-22-6611/dss

Conflicts of Interest: All authors have completed the ICMJE uniform disclosure form (available at https://atm.amegroups.com/article/view/10.21037/atm-22-6611/coif). The authors have no conflicts of interest to declare.

Ethical Statement: The authors are accountable for all aspects of the work in ensuring that questions related to the accuracy or integrity of any part of the work are appropriately investigated and resolved. Animal experiments were performed under a project license (No. SPF2017096) approved by the Animal Care and Use Committee of Guangzhou University of Chinese Medicine, in compliance with the institutional guidelines for the care and use of animals.

References

1. Thong MSY, van Noorden CJF, Steindorf K, et al. Cancer-Related Fatigue: Causes and Current Treatment Options. Curr Treat Options Oncol 2020;21:17.
2. Ebede CC, Jang Y, Escalante CP. Cancer-Related Fatigue in Cancer Survivorship. Med Clin North Am 2017;101:1085-97.
3. Morrow GR. Cancer-related fatigue: causes, consequences, and management. Oncologist 2007;12 Suppl 1:1-3.
4. Ma Y, He B, Jiang M, et al. Prevalence and risk factors of cancer-related fatigue: A systematic review and meta-analysis. Int J Nurs Stud 2020;111:103707.
5. Strebkova R. Cancer-related Fatigue in Patients with Oncological Diseases: Causes, Prevalence, Guidelines for Assessment and Management. Folia Med (Plovdiv) 2020;62:679-89.
6. Tian L, Lin L, Li HL, et al. Prevalence and Associated Factors of Cancer-Related Fatigue Among Cancer Patients in Eastern China. Oncologist 2016;21:1349-54.
7. Dickinson K, Case AJ, Kupzyk K, et al. Exploring Biologic Correlates of Cancer-Related Fatigue in Men With Prostate Cancer: Cell Damage Pathways and Oxidative Stress. Biol Res Nurs 2020;22:514-9.
8. Wilson HE, Stanton DA, Rellick S, et al. Breast cancer-associated skeletal muscle mitochondrial dysfunction and lipid accumulation is reversed by PPARG. Am J Physiol Cell Physiol 2021;320:C577-90.
9. Yang S, Chu S, Gao Y, et al. A Narrative Review of Cancer-Related Fatigue (CRF) and Its Possible Pathogenesis. Cells 2019;8:738.
10. Brownstein CG, Twomey R, Temesi J, et al. Physiological and psychosocial correlates of cancer-related fatigue. J Cancer Surviv 2022;16:1339-54.
11. Hosokawa M, Ito M, Kyota A, et al. Non-pharmacological interventions for cancer-related fatigue in terminal cancer patients: a systematic review and meta-analysis. Ann Palliat Med 2022;11:3382-93.
12. Husebø AML, Dalen I, Søreide JA, et al. Cancer-related fatigue and treatment burden in surgically treated colorectal cancer patients - A cross-sectional study. J Clin Nurs 2022;31:3089-101.
13. Yang C. Effect of Jian Pi Sheng Sui Gao (JPSSG) on fatigue and immune function in patients with non-small cell lung cancer after chemotherapy. Guangzhou University of Chinese Medicine 2019.
14. Zhan PP, Yu L, Lin JT, et al. Clinical Observation of Jianpi Shengsui Herbal Paste in Post-chemotherapy Cancer-related Fatigue. Chinese General Practice 2019;22:1855-9.
15. Xiao ZW, Yang CZ, He CF, et al. Clinical Observation of Jianpi Shengsui Soft Extract for Treatment of Chemotherapy-related Fatigue in Patients with Lung Cancer. Journal of Oncology in Chinese Medicine 2019;1:24-9.
16. Qiao J, Lin LZ, Sun LL. Lin Lizhu's experience in treating cancer-related fatigue with Jian Pi Sheng Sui Gao (JPSSG). Liaoning Journal of Traditional Chinese Medicine 2017;44:1827-9.
17. Zhang R, Zhu X, Bai H, et al. Network Pharmacology Databases for Traditional Chinese Medicine: Review and Assessment. Front Pharmacol 2019;10:123.
18. Guo W, Liu S, Zheng X, et al. Network Pharmacology/Metabolomics-Based Validation of AMPK and PI3K/AKT Signaling Pathway as a Central Role of Shengqi Fuzheng Injection Regulation of Mitochondrial Dysfunction in Cancer-Related Fatigue. Oxid Med Cell Longev 2021;2021:5556212.
19. Jing C, Sun Z, Xie X, et al. Network pharmacology-

based identification of the key mechanism of Qinghuo Rougan Formula acting on uveitis. Biomed Pharmacother 2019;120:109381.

20. Wang Y, Liu Y, Zhang Y, et al. Effects of the polysaccharides extracted from Chinese yam (Dioscorea opposita Thunb.) on cancer-related fatigue in mice. Food Funct 2021;12:10602-14.

21. Zhou YT, Li SS, Ai M, et al. 1,25(OH)(2)D(3) mitigate cancer-related fatigue in tumor-bearing mice: Integrating network pharmacological analysis. Biomed Pharmacother 2020;128:110256.

22. Lee DY, Chun YS, Kim JK, et al. Curcumin Ameliorated Oxidative Stress and Inflammation-Related Muscle Disorders in C2C12 Myoblast Cells. Antioxidants (Basel) 2021.

23. Kim S, Han J, Lee MY, et al. The experience of cancer-related fatigue, exercise and exercise adherence among women breast cancer survivors: Insights from focus group interviews. J Clin Nurs 2020;29:758-69.

24. Yin L, Li N, Jia W, et al. Skeletal muscle atrophy: From mechanisms to treatments. Pharmacol Res 2021;172:105807.

25. Ancoli-Israel S, Liu L, Natarajan L, et al. Reductions in sleep quality and circadian activity rhythmicity predict longitudinal changes in objective and subjective cognitive functioning in women treated for breast cancer. Support Care Cancer 2022;30:3187-200.

26. Chandan G, Kumar C, Chibber P, et al. Evaluation of analgesic and anti-inflammatory activities and molecular docking analysis of steroidal lactones from Datura stramonium L. Phytomedicine 2021;89:153621.

27. Carling D. AMPK signalling in health and disease. Curr Opin Cell Biol 2017;45:31-7.

28. Jia SS, Liu YH. Down-regulation of hypoxia inducible factor-1alpha: a possible explanation for the protective effects of estrogen on genioglossus fatigue resistance. Eur J Oral Sci 2010;118:139-44.

29. Liang B, Zhu YC, Lu J, et al. Effects of Traditional Chinese Medication-Based Bioactive Compounds on Cellular and Molecular Mechanisms of Oxidative Stress.

Oxid Med Cell Longev 2021;2021:3617498.

30. Forman HJ, Zhang H. Targeting oxidative stress in disease: promise and limitations of antioxidant therapy. Nat Rev Drug Discov 2021;20:689-709.

31. Wan JJ, Qin Z, Wang PY, et al. Muscle fatigue: general understanding and treatment. Exp Mol Med 2017;49:e384.

32. Powers SK, Jackson MJ. Exercise-induced oxidative stress: cellular mechanisms and impact on muscle force production. Physiol Rev 2008;88:1243-76.

33. Jelic MD, Mandic AD, Maricic SM, et al. Oxidative stress and its role in cancer. J Cancer Res Ther 2021;17:22-8.

34. Klaunig JE. Oxidative Stress and Cancer. Curr Pharm Des 2018;24:4771-8.

35. Shin Y, Yoo C, Moon Y, et al. Efficient synthesis of frutinone A and its derivatives through palladium-catalyzed C - H activation/carbonylation. Chem Asian J 2015;10:878-81.

36. Lee YJ, Lin WL, Chen NF, et al. Demethylwedelolactone derivatives inhibit invasive growth in vitro and lung metastasis of MDA-MB-231 breast cancer cells in nude mice. Eur J Med Chem 2012;56:361-7.

37. Zhou B, Wang X, Li F, et al. Mitochondrial activity and oxidative stress functions are influenced by the activation of AhR-induced CYP1A1 overexpression in cardiomyocytes. Mol Med Rep 2017;16:174-80.

38. Thelingwani RS, Dhansay K, Smith P, et al. Potent inhibition of CYP1A2 by Frutinone A, an active ingredient of the broad spectrum antimicrobial herbal extract from P. fruticosa. Xenobiotica 2012;42:989-1000.

39. Crozet P, Margalha L, Confraria A, et al. Mechanisms of regulation of SNF1/AMPK/SnRK1 protein kinases. Front Plant Sci 2014;5:190.

40. Hardie DG. AMP-activated protein kinase: a key system mediating metabolic responses to exercise. Med Sci Sports Exerc 2004;36:28-34.

41. Yang C, Zhong ZF, Wang SP, et al. HIF-1: structure, biology and natural modulators. Chin J Nat Med 2021;19:521-7.